An Investigation of LPI Radar Waveforms Classification in RoF Channels

TURKI ALRUBEAAN[1], KHALID ALBAGAMI[1], AMR RAGHEB[ID][2], SAEED ALDOSARI[1], MAJID ALTAMIMI[ID][1], AND SALEH ALSHEBEILI[1,2]

[1]Electrical Engineering Department, King Saud University, Riyadh 11421, Saudi Arabia
[2]KACST-TIC in Radio Frequency and Photonics (RFTONICS), King Saud University, Riyadh 11421, Saudi Arabia

Corresponding author: Amr Ragheb (aragheb@ksu.edu.sa)

ABSTRACT Intensive research has been developed to either design or classify low probability of intercept (LPI) radar signals. These types of signals are used in different sensitive electronic warfare applications such as electronic support, electronic attack, and radar emitter identification. Linear frequency modulation, nonlinear frequency modulation, frequency shift keying, polyphase Barker, polyphase P1, P2, P3, P4 and Frank codes are examples of LPI waveforms. In this paper, we consider the modulation classification problem under the effect of transporting the captured radar signals through radio over fiber channels. Distortions and noise introduced by such channels are likely to affect the performance of LPI classification algorithms. Here, we investigate the accuracy of a recently proposed hierarchical decision-tree automatic modulation classification algorithm for additive white Gaussian noise channels and provide the necessary adjustments when the intercepted radar signals are transmitted over fiber optic channels. The investigation is conducted by simulations and experimental demonstration. The obtained results show that for an 80 km fiber link and noisy intercepted LPI signals, the average identification accuracy reaches more than 98%, at 16 dB optical signal-to-noise ratio.

INDEX TERMS Automatic modulation classification (AMC), low probability of intercept (LPI) radar waveforms, intrapulse, electronic support (ES), electronic attacks (EA).

I. INTRODUCTION

In today's battlefields, most radars, as in surveillance, reconnaissance, and target tracking radars, have to cope with very capable and advanced threats designed to contribute to the degradation of radar performance [1], [2]. Electronic warfare support (ES) interception capabilities, electronic attack (EA) systems, radar warning receivers (RWRs), and antiradiation missiles (ARMs) are examples of such threats [2]. Therefore, radars are required to hide their emissions from hostile receivers, and as such they are called Low Probability of Intercept (LPI) radars [3], [4].

LPI signals can be realized by using wide operational bandwidth, frequency agility, proper power management, antenna sidelobe reduction, and advanced scan patterns [2], [3]. In particular, reducing the radar's peak effective radiated power (ERP) by using some form of pulse compression techniques is a commonly used approach to realize

LPI radar signals. Pulse compression based on intrapulse modulation is very effective in practice, as it leads to a large time-bandwidth product and high radar signal processing gain. Besides, optimization techniques have been exploited and developed, recently, to design radar waveforms that can increase the performance of LPI radar systems [5], [6]. In this regard, the authors in [5] designed and optimized an LPI-based orthogonal frequency division multiplexed (OFDM) waveform with minimum radiated power that can be used in an integrated radar and communication systems. Moreover, efficient radar resource management and scheduling can lead to proper performance in LPI-based distributed radar networks [7], [8].

Nonetheless, radar electronic support measures (ESM) systems play a major role in modern electronic warfare (EW) for the localization and analysis of intercepted radar signals [3]. Indeed, for electronic intelligence (ELINT) receivers, it is essential to classify the intrapulse modulation after signal detection. Thus, automatic modulation classification (AMC) of radar signals has a significant role in

The associate editor coordinating the review of this article and approving it for publication was Jafar A. Alzubi.

distinguishing one threat from another, choosing appropriate algorithms to estimate radar's key parameters, and performing signal deinterleaving [2], [3].

A. RELATED WORK

There has been considerable work on the classification of LPI radar signals under the effect of wireless channel [3], [9]–[15]. Receivers with AMC processing algorithms usually perform two main steps: the signal preprocessing and the classification. In the first step, certain parameters of the transmitted signal are estimated/extracted (e.g. carrier frequency, time of arrival, pulse width, signal power, etc.). In the second step, intelligent classification algorithms are applied, possibly using two approaches: the likelihood-based (LB) approach and feature-based (FB) approach [16], [17]. The former approach is optimal in certain criteria but suffers from heavy computational complexity [10]. In contrast, the FB algorithms are not optimal but more suitable for real-time implementation. They work on extracting features from the received signal and then applying these features to a classifier.

Classifiers based on hierarchical decision trees (HDTs), where a series of questions that lead to a class label is applied to the extracted features, have been proposed in the literature. These classifiers are non-parametric in the sense that there are no underlying assumptions about the distribution of data under consideration. The works of [9]–[12] belong to this type of classifiers. In particular, the authors of [9] used the generalized time-frequency representation of Zhao, Atlas and Marks (ZAM-GTFR) to extract features pertaining to five types of radar signals (monopulse, linear frequency modulation (LFM), binary phase shift keying (BPSK), binary frequency shift keying (2FSK), and 4FSK). The ZAM-GTFR is characterized by simultaneously preserving the property of finite-time support, strengthening spectral peaks, and smoothing cross-terms. At low SNR, it shows some advantageous performance over other TFRs. In [10], classification of four possible types of modulations are considered: the nonintrapulse modulation (NM), LFM (ascending or descending), FM, and PSK with orders 2, 4, and 8. Simple features extracted from the signal's instantaneous phase and frequency are used to develop a low-computational-complexity radar AMC suitable for real-time Field Programmable Gate Array (FPGA) implementation. This simplicity in extracting features, however, comes at the expense of the requirement of a higher SNR in comparison with more complex features. In [11], the linear/nonlinear frequency modulation (L/NFM), binary frequency shift keying (BFSK), phase modulation (PM) (polyphase Barker and polyphase codes) are classified using the HDT approach. In this work, the features are derived using Radon ambiguity transform (RAT), Radon-Wigner Ville distribution (WVD), and fractional Fourier transform (FRT). In [12], a new wideband receiver based on modulated wideband converter and compressed sampling is developed for the purpose of intercepting and classifying LPI radar signals. The short-time Fourier transform (STFT) and spectrum energy
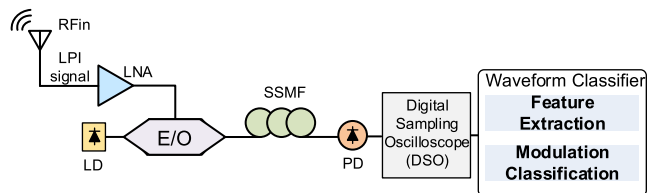

FIGURE 1. Block diagram of the intrapulse modulation classification system. LNA: Low noise amplifier, LD: Laser diode, E/O: Electro/optic modulator, SSMF: Standard signal mode fiber, PD: Photodiode.

focusing rate tests are employed to classify phase modulation signals and frequency modulation signals. The proposed receiver consists of a reduced number of sub-Nyquist sampling branches, thereby, it saves storage space and reduces computational complexity.

Supervised learning has also been attempted in literature for radar signal classification. In such an approach, the algorithm first learns from labeled data to infer a model, which can be used for classifying new examples [13]. In [14], the authors utilized supervised learning to classify eight types of radar signals: LFM, discrete frequency codes (Costas codes), binary phase, and Frank, P1, P2, P3, and P4 polyphase codes. Features extracted from second order statistics, instantaneous signal properties, and Wigner and Choi-Williams time-frequency distributions are applied to a parallel classifier structure based on multilayer perceptron (MLP) networks. Equipped with sigmoidal hidden unit activation functions, MLP can provide universal approximators for any decision boundary to an arbitrary accuracy [14]. In [15], eight types of LPI waveforms (LFM, Costas codes, BPSK, Frank code, and P1-P4) have been considered for classification. Features extracted from the signal directly (e.g. second order statistics, power spectral density, etc.) and those obtained from the 2D image of a time-frequency distribution are applied to Elman neural network (ENN). This network has a feedback, hence, its recognition rate is relatively high at low SNR. In [16], the authors have considered twelve pulse compression waveforms, including all polyphase and polytime waveforms. They used the time-frequency images (TFIs) produced by time-frequency analysis (TFA) as inputs to a convolutional neural network (CNN). This network is a deep learning network assigning learnable weights and biases to various aspects/objects in TFI images. CNN is capable of capturing the spatial and temporal dependencies of the input images, which leads to improvement in classification performance.

B. PAPER'S CONTRIBUTION

All of the previously mentioned AMC techniques have been developed under the assumption of additive white Gaussian noise (AWGN) channels. In this paper, we investigate the performance of an AMC technique under the assumption of signaling over fiber optic channels. Fig. 1 shows the schematic diagram of the proposed radio over fiber (RoF) model. A continuous wave laser diode (LD) is fed into a Mach-Zehnder modulator (MZM) which modulates the optical carrier with the intercepted LPI signals. A low noise

amplifier (LNA) is used to enhance the LPI signal power. The obtained optical double side band (DSB) signal, at the MZM's output, is transmitted over a fiber channel using a standard single mode fiber (SSMF). The receiver side comprises a photodetector which converts the LPI signal back to the electrical domain by heterodyning, an electrical sampling oscilloscope that analyzes and generates the LPI signal samples, and an offline waveform classifier which includes feature extraction and modulation classification. Note that receivers utilized for radar signal interception are usually located far away from the command and control centers, therefore, it is necessary to transport the radar signal through transmission medium efficient for long distances. Fiber optic channel is a good candidate for radio and millimeter wave signal transmission and distribution [18]. It comprises many advantages such as low transmission loss, immunity to electromagnetic interference, and low latency. Nonetheless, fiber optic channel suffers from linear and nonlinear impairments that affect the radio signal transmission [19]–[21]. This includes amplified spontaneous emission (ASE) noise, chromatic dispersion (CD), polarization dependent loss (PDL), etc.

In this paper, we study the performance of the recently published AMC technique presented in [11] when the captured LPI radar signals are transported through fiber optic channels, as shown in Fig.1. This AMC technique is based on well-known transform operations and a simple thresholding technique. In particular, it has an HDT structure and performs well even at low SNR values. The performance of this AMC algorithm is investigated in terms of classification accuracy under the effect of AWGN, ASE noise, and CD. We consider the classification for the following set of modulations: LFM, FSK, polyphase P1, P2, P3, P4 and Frank code. The modulation features are extracted using Wigner distribution, Radon transform, and ambiguity function. Note that the distortions and noise introduced by fiber optic channels are likely to affect the performance of LPI waveforms classifier; hence, the HDT thresholds need to be properly adjusted. Here, we provide the necessary adjustments and evaluate the effectiveness of the modified AMC algorithm for radio over fiber (RoF) channels using both simulations and experimental demonstration. The obtained results show an average identification accuracy of more than 98% for noisy intercepted LPI radar waveforms at 80 km fiber transmission and 16 dB optical signal to noise ratio (OSNR).

The remainder of this paper is organized as follows. Section II provides the implementation approach of the LPI waveform classification algorithm. LPI waveform classification for optical channels is discussed in Section III using simulation and experimental work. Section IV provides concluding remarks.

II. LPI RADAR WAVEFORMS CLASSIFICATION

Consider the discrete time complex samples of the received intercepted signal $y[n]$ given by [12]

$$y[n] = x[n] + w[n], \quad 0 \le n \le N - 1 \quad (1)$$

where

$$x[n] = A \exp(j(2\pi f[n]n + \phi[n])) \quad (2)$$

is the original transmitted LPI signal with a constant amplitude A in the pulse duration with N samples and an instantaneous frequency and phase given by $f[n]$ and $\phi[n]$, respectively. $w[n]$ is the additive white Gaussian noise (AWGN) of zero mean and variance σ^2.

• For the frequency modulated LPI signals, $\phi[n]$ is constant and the instantenous frequency of the LFM signal is given by,

$$f[n] = f_c + rn \quad (3)$$

where f_c is the RF carrier frequcny and r is the LFM's chirp rate. For FSK signals the instantenous frequency hops over a set of predefined frequencies equal to the FSK modulation order.

• For the polyphase coded LPI signals, $f[n]$ is constant and $\phi[n]$ is the nth element of the vector $\boldsymbol{\theta}$ defined as

$$\boldsymbol{\theta} = \text{vect}(\boldsymbol{\Psi}) \otimes \boldsymbol{u} \quad (4)$$

where $\boldsymbol{\Psi} \in R^{K \times K}$ is the phase matrix of Frank, P1, and P2 codes with entries defined in (5) - (7). For P3 and P4 codes, $\boldsymbol{\Psi}$ is a $1 \times L$ vector with entries defined in (8) and (9). vect($\boldsymbol{\Psi}$) is a row vector obtained by cascading the rows of $\boldsymbol{\Psi}$ beside each other. The symbol $\otimes$ denotes Kronecker product, and $\boldsymbol{u}$ is an all ones vector with dimension D, which depends on the oversampling and number of cycles per phase factors. The entries of $\boldsymbol{\Psi}$ are given by [16]

$$\text{Frank}: \psi_{i,j} = \frac{2\pi}{K}(i-1)(j-1) \quad (5)$$

$$\text{P1}: \psi_{i,j} = \frac{-\pi}{K}[(K-(2j-1))][(j-1)K+(i-1)] \quad (6)$$

$$\text{P2}: \psi_{i,j} = \frac{-\pi}{2K}[2i-1-K][2j-1-K] \quad (7)$$

$$\text{P3}: \psi_i = \frac{\pi}{L}(i-1)^2 \quad (8)$$

$$\text{P4}: \psi_i = \frac{\pi}{L}(i-1)^2 - \pi(i-1) \quad (9)$$

where K is the code order, L is a compression order, and i and j are integers with values ranging from 1 to K (L) for P1, P2, and Frank (P3 and P4) codes. Fig.2 shows the phase shifts of the LPI polyphase coded signals for $K = 8$ and $L = 64$.

The classification process starts by extracting the necessary waveform features from the intercepted signal. According to [11], the LPI signal can be classified as follows.

A. CLASSIFICATION OF FREQUENCY SHIFT KEYING (FSK) SIGNALS

First, we classify whether the received signal is an FSK modulated signal or a coded waveform. This can be achieved by evaluating the Fourier transform (FT) of the intercepted signal. Fig. 3 shows the normalized spectrum of FSK and Frank coded waveforms. We notice that the number of peaks that are within 3dB of the normalized amplitude is one for the
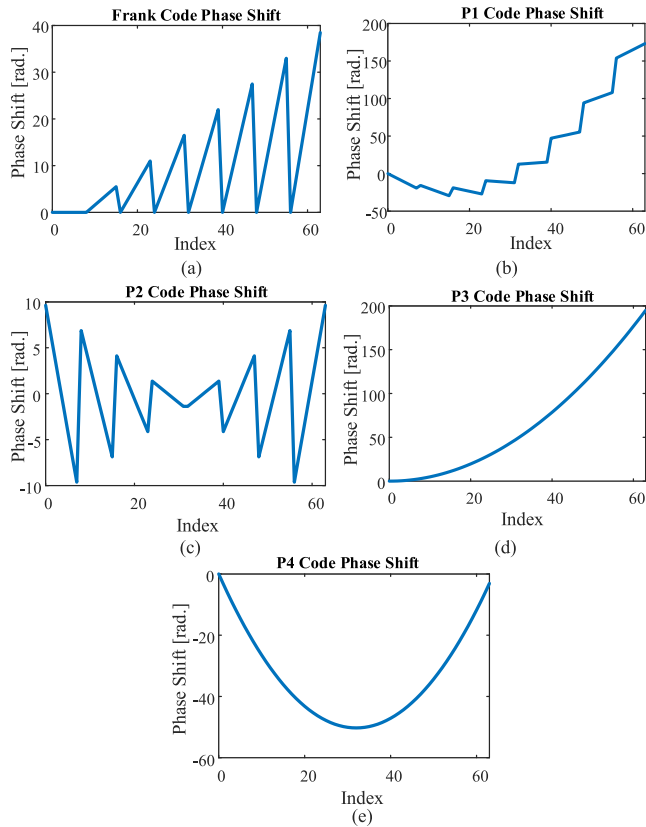
FIGURE 2. Phase shift of Polyphase coded signals. (a) Frank, (b) P1, (c) P2, (d) P3, and (e) P4.
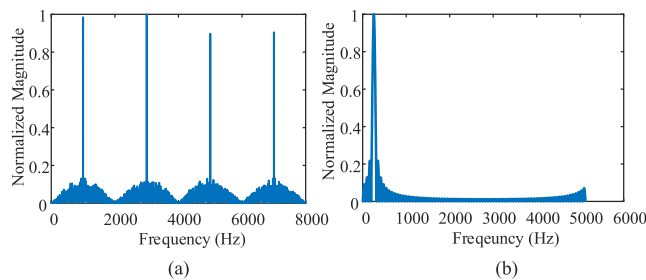

FIGURE 3. Comparison between normalized FT of (a) FSK and (b) Frank-coded signals.

polyphase signals and higher than or equal to 2 for the case of FSK.

B. CLASSIFICATION OF FREQUENCY MODULATED SIGNALS

In this test, the goal is to differentiate between the linear frequency modulated (LFM) signals and other polyphase signals. The classification of LFM requires the use of Ambiguity Function (AF) and Radon Transform (RT) [11]. The energy of AF of LFM signals is concentrated along a line passing through the origin of the ambiguity plane. RT is then performed to compute the integral over lines passing through the origin of the ambiguity plane. This leads to the conversion of high-energy lines in ambiguity plan into high intensity spots in the polar domain. An example of this transformation is
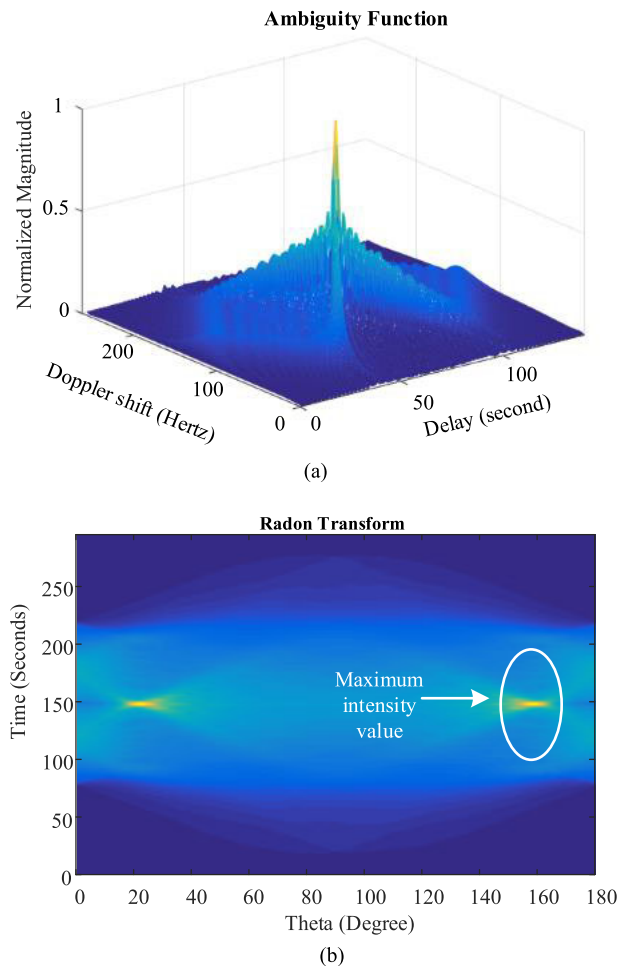

FIGURE 4. Conversion of linear patterns present in ambiguity plane into high intensity spots in the polar domain for LFM. (a) Ambiguity function. (b) Radon transform.

shown in Fig. 4 and Fig. 5 for LFM and P3 code, respectively. The 2-D plot of RT can be viewed as a matrix. Let $\hat{c}$ denote the column where the highest intensity value is located. If the number of intensity peaks belonging to the column $\hat{c}$ is equal to one, then the signal is classified as an LFM signal; otherwise, it is classified as polyphase signal.

C. CLASSIFICATION OF POLYPHASE SIGNALS

In this test, the aim is to differentiate between the polyphase signals; Frank code, P1, P2, P3, and P4. In this regard, we evaluate the Wigner-Ville Distribution function (WDF) to calculate the instantaneous frequency (IF), corresponding to the frequency where the WDF is maximum at a particular instant of time. The resulting IF is smoothed using a median filter. By plotting the IF of different polyphase signals, we notice that Frank and P3 coded signals have maximum IF variation which occurs in the middle, whereas P1, P2, and P4 coded signals have the maximum variation occurring at the end of their IF plot. Fig. 6 shows the IF of Frank and polyphase coded signals.
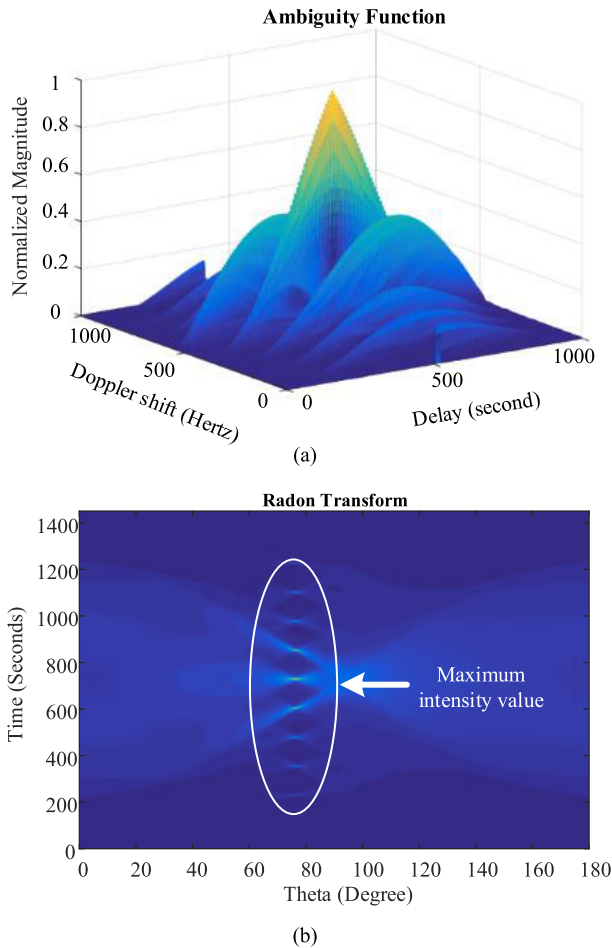
Ambiguity Function

(a)

Radon Transform

Maximum
intensity value

(b)

FIGURE 5. Conversion of linear patterns present in ambiguity plane into high intensity spots in the polar domain for P3 code. (a) Ambiguity function. (b) Radon transform.

Polyphase P1 code

(a)

Polyphase P2 code

(b)

Polyphase P3 code

(c)

Polyphase P4 code

(d)

Frank code

(e)

FIGURE 6. The instantaneous frequency (IF) of (a) P1, (b) P2, (c) P3, (d) P4, and (e) Frank coded polyphase signals.

(a)

(b)

FIGURE 7. Comparison between the histogram of (a) Frank and (b) P4-coded signals.

Therefore, polyphase signals can be divided into two categories according to their IFs. In particular, the IFs of P1, P2, and Frank coded signals have a stair-like shape, whereas the IFs of P4 and P3 signals are approximately linear; see Fig. 6. Based on this observation, the histogram of IF can then be used to further differentiate between these different signals. Obviously, the stair-shaped signals have higher histogram bin values since the value of each step is repeated many times, whereas, the signals with the shape of climbing straight line will have lower histogram bin values since their values are rarely repeated, as shown in Fig. 7. The histogram bins are then classified to be belonging to either category of signals by comparing their values to a threshold, which is determined through the experimental fine-tuning process. Note that the slope of stair-shaped IF can be used to differentiate between P1 and P2-coded signals. For P1-coded signal, the stair-shaped IF is climbing (i.e., it has a positive slope), whereas for P2-coded signal, it is declining (i.e., it has a negative slope), as shown in Fig. 6. Algorithm 1 summarizes the classification algorithm under consideration. In Table I, we present the correct classification percentage results of polyphase coded signals and frequency modulated waveforms under AWGN effect for SNR values of −2 and −10 dB, respectively.
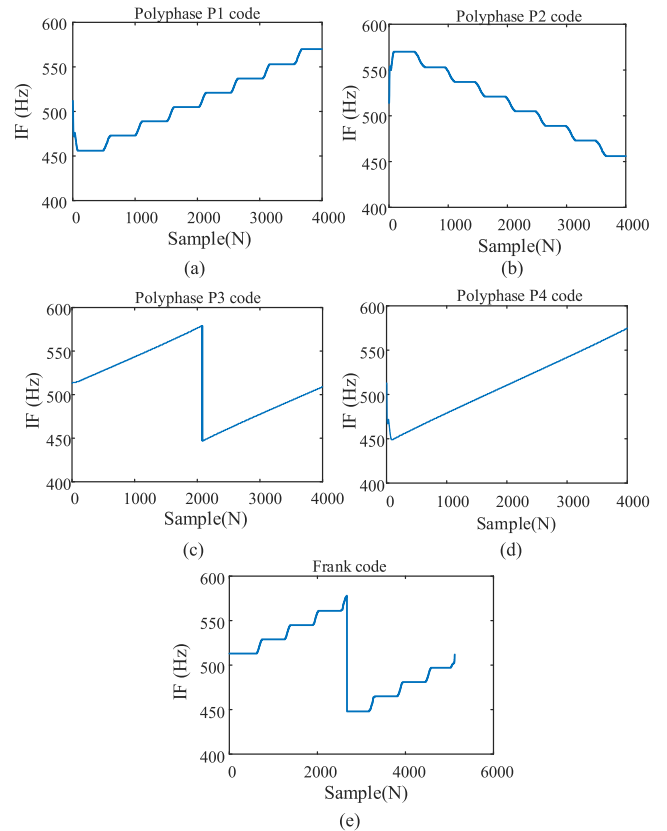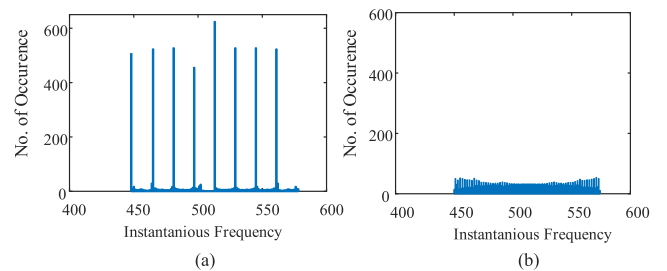
III. LPI WAVEFORM CLASSIFICATION IN ROF CHANNELS

In this section, we investigate the effect of transmitting the LPI radar waveforms through a fiber cable, prior to classification. The investigation will be performed first by simulation and then by experimental demonstration.

A. SIMULATION INVESTIGATION

The *VPItransmissionMaker* 9.9 platform has been used here to simulate the responses of all different components in the optical system model of Fig. 1. Table 2 shows the simulated parameters of the RoF optical setup.

1) EFFECT OF CD AND ASE ON NOISELESS LPI SIGNAL

The front end receiver, shown in Fig. 1, comprises a simple optical amplitude modulator (AM) that generates an optical

Algorithm 1 LPI Classification Algorithm

Step 1. Initialization: Perform signal acquisition and digitization.
Set Th1 = 2, Th2 = 1, and Th3 = 2.

Step 2. FSK Test: Perform FT.
If the no. of 3dB peaks is greater than or equal to Th1 then FSK modulation.
Otherwise, go to Step 3.

Step 3. LFM Test: Perform AF and RT.
If the number of maximum intensity values is equal to Th2 then LFM modulation.
Otherwise, go to Step 4.

Step 4. Polyphase Test 1: Evaluate WDF and determine IF.
If the maximum spectral variation occurs in the middle, then Frank
or P3 code modulations and go to Step 5.
Otherwise, P1, P2, or P4 code modulations and go to Step 6.

Step 5. Polyphase Test 2: Obtain IF histogram.
If no. of histogram bins is greater than Th3 then Frank code modulation.
Otherwise, P2 code modulation.

Step 6. Polyphase Test 3: Obtain IF histogram.
If no. of histogram bins is greater than Th.3, then P4 code modulation.
Otherwise, P1 or P2 code modulation and go to Step 7.

Step 7. Polyphase Test 4: Evaluate IF slope.
If slope > 0 then P1 code modulation. Otherwise, P2 modulation

TABLE 1. AWGN channel correct classification simulation results.

Modulation	SNR (dB)	Percent of Correct Classification (%)
P1 code	-2	95
P2 code	-2	87
P3 code	-2	76
P4 code	-2	92
Frank code	-2	100
FSK (M=4)	-10	98
LFM	-10	99

TABLE 2. Parameters of the RoF optical setup.

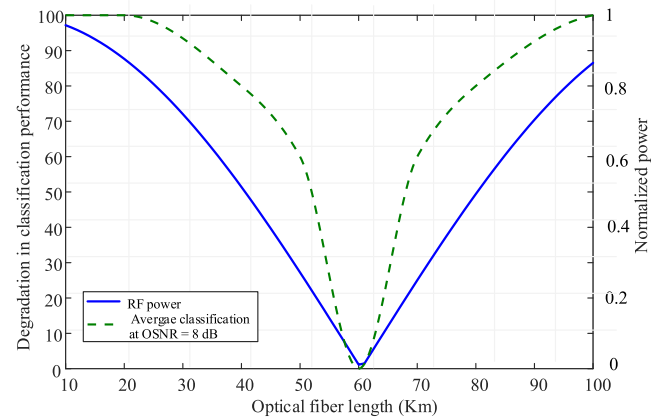| Modulation	Polyphase codes	LFM
Code element duration / Pulse duration	32 ns	1024 ns
Bandwidth	62 MHz	80 MHz
Carrier frequency	8 GHz (X-band)	
Noise	AWGN + ASE	
SNR	-2 dB	-10 dB
OSNR	4 to 20 dB, 2dB step	
Fiber length (L)	80 km	
Fiber dispersion (D)	16 $\mu s/m^2$	
Fiber attenuation (α)	0.2 dB/km	

FIGURE 8. Comparison between degradation in RF power and classification performance vs. optical fiber length, at OSNR = 8 dB.
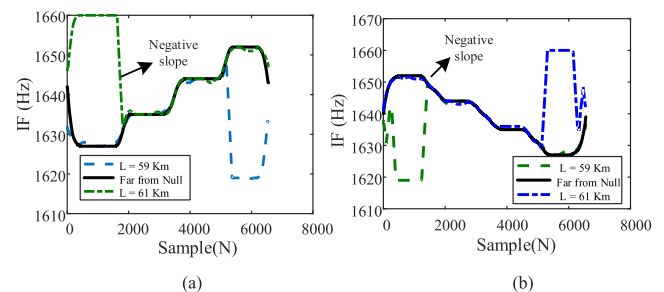

FIGURE 9. IF of (a) P1 and (b) P2-coded signal at lengths near and far form the 1st CD effect.

double side band (ODSB) signal. At the receiver side, each single-side band is beaten with the laser carrier to produce the captured radar signal. However, due to fiber CD effect, each side band will experience different phase shift that causes degradation in the re-generated RF power [21]. In our study, the first CD effect (null) occurs when the fiber length equals $L = 59.5$ km. Fig. 8 shows the degradation in RF power (right axis) versus optical fiber length for a radar signal in X-band ($f_{RF} = 8$ GHz). Also, the classification performance (left axis) versus fiber length is shown in Fig. 8, at OSNR = 8 dB.

To investigate the effect of CD, Fig. 9 shows the deviation in the IF of the polyphase signals (P1 and P2 coded signal) under the effect of CD. This causes the classifier to be confused between P1 and P2 codes since the distinct features between P1-coded signal and P2-coded signal are the climbing (positive slope) and declining stair-shaped IF (negative slope). Same behavior is noticed between the Frank-coded and P1-coded signals, as the maximum variation occurs in the middle for the Frank-codded signal, but due to CD effect (IF shift), the maximum variation no longer occurs in the middle, which causes the confusion between both signals (Frank-coded and P1-coded), see Fig 10. Table 3 shows the confusion matrix for the correct modulation classification at $L = 61$ km. In this matrix, the off-diagonal entries represent the number of times a modulation scheme is misclassified by other modulation schemes, whileas the diagonal entries represent the number of correct classifications.

To mitigate the effect of CD, a correction factor (β_L) is added to the threshold parameter of the classifier.
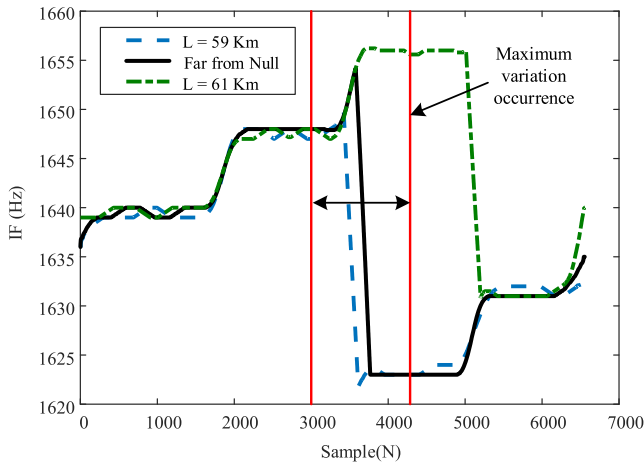
FIGURE 10. IF of Frank-coded signal at lengths near and far from the 1st CD effect.

TABLE 3. Confusion matrix for correct modulation calssification at *L* = 61 km, without CD correction factor.

	P1 Code	P2 Code	P3 Code	P4 Code	Frank Code	LFM
P1 Code	0%	100%	0%	0%	0%	0%
P2 Code	0%	100%	0%	0%	0%	0%
P3 Code	0%	0%	80%	0%	20%	0%
P4 Code	0%	0%	0%	100%	0%	0%
Frank Code	100%	0%	0%	0%	0%	0%
LFM	0%	0%	0%	0%	0%	100%

TABLE 4. Confusion matrix for correct modulation calssification at *L* = 61 km, with CD correction factor.

	P1 Code	P2 Code	P3 Code	P4 Code	Frank Code	LFM
P1 Code	100%	0%	0%	0%	0%	0%
P2 Code	0%	100%	0%	0%	0%	0%
P3 Code	0%	0%	100%	0%	0%	0%
P4 Code	0%	0%	0%	100%	0%	0%
Frank Code	0%	0%	0%	0%	100%	0%
LFM	0%	0%	0%	0%	0%	100%

This factor corresponds to the shift occurring in the IF of the polyphase signals, which varies with different fiber lengths. Table 4 shows the improved confusion matrix after adding a CD's correction factor to the classifier. For instance, the correction factor is 1300 samples for fiber length equals 61 Km.

Next, we consider the ASE noise effect by testing the classifier at different values of OSNR starting from 4 dB to 20 dB with 2 dB step, under the assumption that the intercepted radar signal is noiseless. OSNR range has been chosen according to the typical values of optical fiber transmission systems. Fig. 11 compares the classification performance of different LPI waveforms versus OSNR, at 80 km fiber length. We notice that the classification performance becomes acceptable as OSNR reaches ≈ 10 dB. For instance, in Fig. 12 we show the IF of P1 and P3 coded signals at OSNR = 8 dB.

2) EFFECT OF CD AND ASE ON NOISY LPI RADAR SIGNALS
So far, we have studied the effect of OSNR on noiseless intercepted LPI radar signals passing through the optical
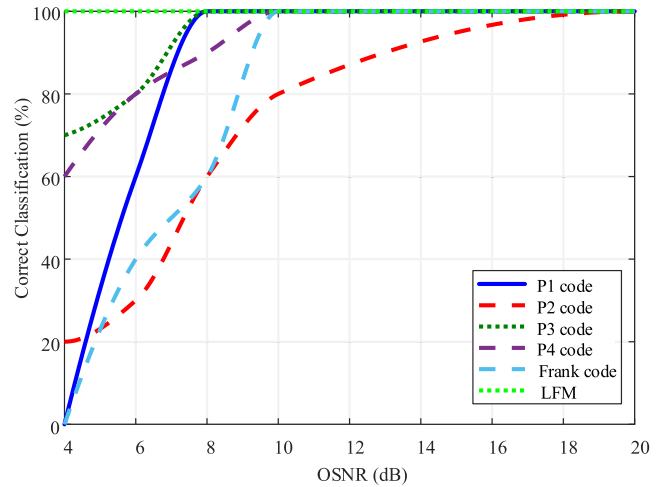

FIGURE 11. Classification performance vs. OSNR of noiseless intercepted radar signal at *L* = 80 km.
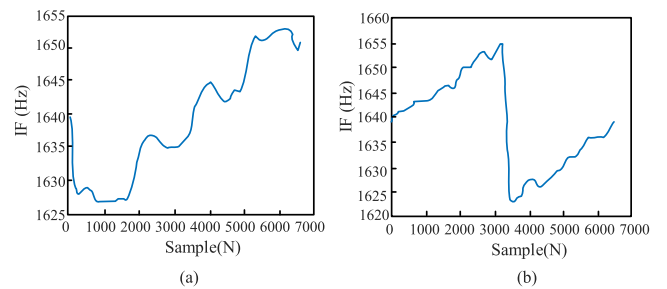

FIGURE 12. (a) IF of P1-coded signal and (b) IF of P3-coded signal, at OSNR = 8 dB.

fiber cable. Here, we study the effect of both AWGN and OSNR effects together, according to the simulation parameters, given in Table I. Fig. 13 shows the classification performance versus OSNR, with 80 km fiber length, for polyphase codes and LFM signals at SNR = −2 and −10dB, respectively. We can clearly see that the classification performance has degraded due to the joint presence of both AWGN and ASE noise.

B. EXPERIMENTAL DEMONSTRATION
In this section, we verify the simulation results by experimentally demonstrating the RoF transmission system. The process of verification is implemented by considering wireless channel with AWGN and optical channel with CD and ASE noise. Fig. 14 shows the experimental setup of the optical system. A tunable laser (Keysight N7714A) source is used to generate a 1550 nm optical signal, which is utilized as a carrier in the optical transmission system. Then, the LPI radar signals are generated and loaded into Keysight M9180A arbitrary waveform generator (AWG). The optical carrier is modulated by the upconverted radar signal (using Keysight VSG E8267D), in a 40 GHz MZM (EOspace AZ-DV5-40-PFU-SFU-LV). The MZM has a switching voltage (Vπ) of 4.6 volts and it is biased at its quadrature transmission
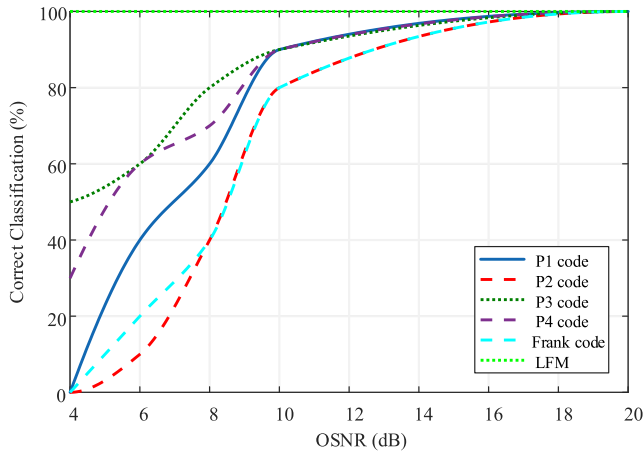
FIGURE 13. Classification performance vs. OSNR at $L = 80$ km for noisy LPI signals.
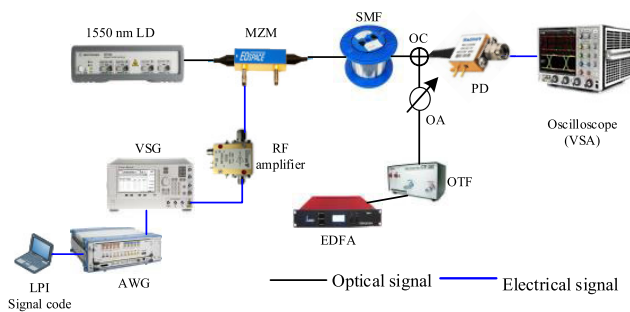

FIGURE 14. Experimental setup of the demonstrated RoF transmission system. LD: Laser diode, AWG: Arbitrary waveform generator, VSG: Vector signal generator, MZM: Mach Zehnder modulator, SMF: Single mode fiber, OC: Optical coupler, EDFA: Erbium doped fiber amplifier, OTF: Optical tunable filter, OA: Optical attenuator, PD: Photodetector, VSA: Vector signal analyzer.

TABLE 5. Signals parameters for experimental setup.

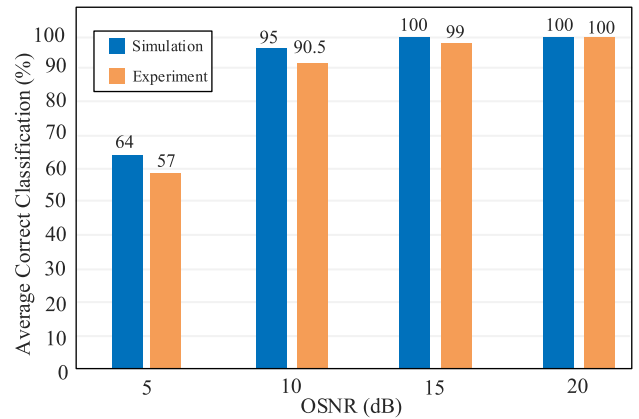| Modulation	Polyphase codes	LFM
Code element duration / Pulse duration	32 ns	1024 ns
Bandwidth	62 MHz	80 MHz
Carrier frequency	8 GHz (X- band)	
Noise	ASE	
OSNR	5 to 20 dB, 5dB step	

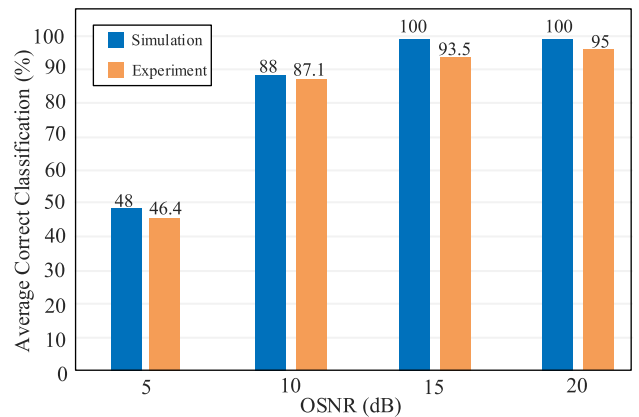**FIGURE 15.** Average correct classification in back-to-back optical system under ASE noise only.

FIGURE 16. Average correct classification in back-to-back optical system under both AWGN and ASE noises.

point (Q-point) to work as an amplitude modulator (AM). The modulated carrier is then transmitted over a standard single mode fiber (Corning SSMF-28) of 80 km length and fiber dispersion and attenuation parameters equal to 16 μs/m^2 and 0.2 dB/km, respectively. The ASE noise is generated using a C-band Erbium-doped fiber amplifier (Amonics-AEDFA-18-R-FA) and added to the modulated optical signal using a 50:50 optical coupler (OC). At the receiver side, a broad bandwidth photodetector (Finisar XPDV3120R) is used to demodulate the optical signal and recover the electrical radar signal back. A 32 GHz digital sampling oscilloscope (Keysight-DSOX93294A) is used to analyze the received radar waveforms. The parameters used in the experiment are shown in Table V.

First, we considered a back-to-back optical transmission system and investigated the effect of AWGN and ASE noises. Fig.15 shows the classification performance in case of ASE noise only. The OSNR values change from 5 to 20 dB with a step size of 5 dB. The experimental investigation shows a correct classification exceeding 90% at OSNR $\geq$ 10 dB.

Then, we considered both ASE and AWGN noise simultaneously. The polyphase codes and the frequency modulated signals are generated with SNR of -2 and -10 dB, respectively. The OSNR values are changed as in the previous study. The experimental results, shown in Fig. 16, show that the classification accuracy exceeds 90% for OSNR $\geq$ 15 dB. Finally, we investigated the CD effect using optical transmission, where a comparison between the simulation and experimental investigations, of the classifier performance, is shown in Fig. 17 for a fiber cable length of 80 km. It is evident from Fig. 17 that a good agreement between simulation and experiment results can be noticed at various OSNR values. The classifier reaches an average recognition accuracy of 90% at 10 dB OSNR.
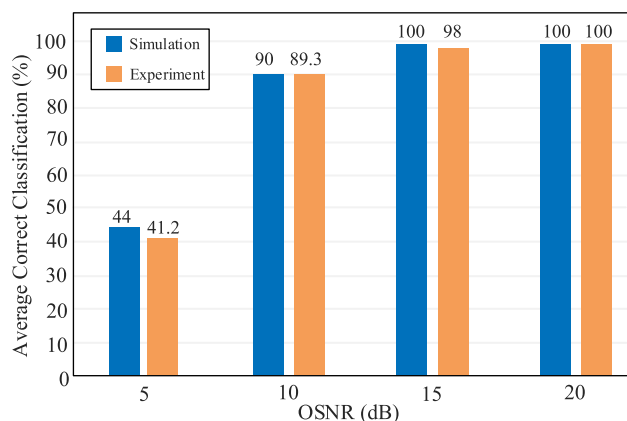
FIGURE 17. Average correct classification in optical transmission at *L* = 80 km under ASE noise and CD effect.

IV. CONCLUSION

In real situations, intercept receivers are usually placed away from a main command and control center, which makes it necessary to transmit the intercepted signal over a communication medium. This paper aims to study the optical fiber transmission medium and its effect on the intercepted LPI radar signals. In particular, both simulations and experiments have been considered for evaluating the performance of a recently proposed automatic classification algorithm in the presence of AWGN, CD, and ASE noise. Throughout this investigation, there is always an excellent agreement between the simulation and experimental results. Results show that by properly adjusting the CD's correction factor it would be possible to mitigate the effect of CD, and the algorithm will behave as in AWGN case. In particular, for noiseless intercepted LPI signals transmitted over 80 km fiber link, the identification accuracy reaches 100% at 10 dB OSNR for LFM, P1, P3, P4, and Frank code. However, for noisy LPI signals, the 100% accuracy is reached for all modulations at a higher OSNR (18dB).

This paper has considered an HDT-based AMC classifier, which is very attractive for real-time applications when radar signals are transmitted over optical channels. For future work, researchers could study more advanced classifiers to further enhance the classification accuracy, specifically, for intercepted LPI signals with low SNR values and consider their hardware implementation to meet the constraints of practical systems.

REFERENCES

[1] S. Samadi, M. R. Khosravi, J. A. Alzubi, O. A. Alzubi, and V. G. Menon, "Optimum range of angle tracking radars: A theoretical computing," *Int. J. Elect. Comput. Eng.*, vol. 9, no. 3, pp. 1765–1772, Jun. 2019.

[2] A. Denk, "Detection and jamming low probability of intercept (LPI) radars," M.S. thesis, Naval Postgraduate School, Monterey CA, USA, 2006.

[3] R. G. Wiley, *ELINT: The Interception and Analysis of Radar Signals*. Norwood, MA, USA: Artech House, 2006.

[4] A. G. Self and B. G. Smith, "Intercept time and its prediction," *IEE Proc. F-Commun., Radar Signal Process.*, vol. 132, no. 4, pp. 215–220, Jul. 1985.

[5] C. Shi, F. Wang, S. Salous, and J. Zhou, "Low probability of intercept-based optimal OFDM waveform design strategy for an integrated radar and communications system," *IEEE Access*, vol. 6, pp. 57689–57699, 2018.

[6] C. Shi, F. Wang, M. Sellathurai, J. Zhou, and S. Salous, "Power minimization-based robust OFDM radar waveform design for radar and communication systems in coexistence," *IEEE Trans. Signal Process.*, vol. 66, no. 5, pp. 1316–1330, Mar. 2018.

[7] Z. Zhang and Y. Tian, "A novel resource scheduling method of netted radars based on Markov decision process during target tracking in clutter," *EURASIP J. Adv. Signal Process.*, vol. 2016, no. 1, p. 16, Dec. 2016.

[8] C. G. Shi, F. Wang, S. Salous, and J. J. Zhou, "Joint transmitter selection and resource management strategy based on low probability of intercept optimization for distributed radar networks," *Radio Sci.*, vol. 53, no. 9, pp. 1108–1134, Sep. 2018.

[9] D. Zeng, X. Zeng, G. Lu, and B. Tang, "Automatic modulation classification of radar signals using the generalised time-frequency representation of Zhao, Atlas and Marks," *IET Radar, Sonar Navigat.*, vol. 5, no. 4, pp. 507–516, Apr. 2011.

[10] V. Iglesias, J. Grajal, P. Royer, M. A. Sanchez, M. Lopez-Vallejo, and O. A. Yeste-ojeda, "Real-time low-complexity automatic modulation classifier for pulsed radar signals," *IEEE Trans. Aerosp. Electron. Syst.*, vol. 51, no. 1, pp. 108–126, Jan. 2015.

[11] T. R. Kishore and K. D. Rao, "Automatic intrapulse modulation classification of advanced LPI radar waveforms," *IEEE Trans. Aerosp. Electron. Syst.*, vol. 53, no. 2, pp. 901–914, Apr. 2017.

[12] T. Chen, L. Liu, and X. Huang, "LPI radar waveform recognition based on multi-branch mwc compressed sampling receiver," *IEEE Access*, vol. 6, pp. 30342–30354, 2018.

[13] C. M. Bishop and G. Hinton, *Neural Networks for Pattern Recognition*. Oxford, U.K.: Oxford Univ. Press, 1995.

[14] J. Lundén and V. Koivunen, "Automatic radar waveform recognition," *IEEE J. Sel. Topics Signal Process.*, vol. 1, no. 1, pp. 124–136, Jun. 2007.

[15] M. Zhang, L. Liu, and M. Diao, "LPI radar waveform recognition based on time-frequency distribution," *Sensors*, vol. 16, no. 10, pp. 1682–1701, Oct. 2016.

[16] S.-H. Kong, M. Kim, L. M. Hoang, and E. Kim, "Automatic LPI radar waveform recognition using CNN," *IEEE Access*, vol. 6, pp. 4207–4219, 2018.

[17] O. A. Dobre, A. Abdi, Y. Bar-Ness, and W. Su, "Survey of automatic modulation classification techniques: Classical approaches and new trends," *IET Commun.*, vol. 1, no. 2, pp. 137–156, Apr. 2007.

[18] M. A. Esmail, A. Ragheb, H. Seleem, H. Fathallah, and S. Alshebeili, "Radar signal transmission and switching over optical networks," *Opt. Commun.*, vol. 410, pp. 385–388, Mar. 2018.

[19] G. Han, S. Li, H. Wang, X. Xue, and X. Zheng, "A microwave photonics equalizer for overcoming dispersion-induced distortions on wideband signals in radio-over-fiber links," *J. Lightw. Technol.*, vol. 37, no. 3, pp. 736–743, Feb. 1, 2018.

[20] L. Guesmi and M. Menif, "Modulation formats recognition technique using artificial neural networks for radio over fiber systems," in *Proc. 17th Int. Conf. Transparent Opt. Netw. (ICTON)*, Budapest, Hungary, Jul. 2015, pp. 1–4.

[21] J. Ma, J. Yu, C. Yu, X. Xin, J. Zeng, and L. Chen, "Fiber dispersion influence on transmission of the optical millimeter-waves generated using LN-MZM intensity modulation," *J. Lightw. Technol.*, vol. 25, no. 11, pp. 3244–3256, Nov. 2007.

TURKI ALRUBEAAN received the B.S. degree in electrical engineering from King Saud University (KSU), Riyadh, Saudi Arabia, in 2018. He is currently a Network-Planning Engineer with Saudi Telecom Company (STC), where he is involved in the domain of telecommunication and networks.

KHALID ALBAGAMI received the B.Sc. (Eng.) degree (Hons.) in electrical engineering telecommunication track from King Saud University, in 2018. He is currently a Solution Architect with Ericsson AB, where he is involved in the domain of telecommunication and networks.

AMR RAGHEB received the B.S. (Hons.) and M.Sc. degrees from Tanta University, Egypt, in 2001 and 2007, respectively, and the Ph.D. degree from King Saud University, Riyadh, Saudi Arabia, in 2015, all in electrical engineering. He was a Teaching Assistant with Tanta University, from 2003 to 2008. He was a Teaching Assistant with King Saud University, from 2010 to 2015. He has over seven years of experience with the Photonics Telecommunication Laboratory. He is currently an Assistant Professor with King Saud University. His research interest include photonic-microwave integration, quantum dash-based lasers, free space optical communications, coherent optical receivers, multi-format high speed optical transmitter, and passive optical networks.

SAEED A. ALDOSARI received the B.S. and M.S. degrees in electrical engineering from King Saud University, Riyadh, Saudi Arabia, in 1994 and 2000, respectively, and the Ph.D. degree in electrical and computer engineering from Carnegie Mellon University, Pittsburgh, PA, USA, in 2005. He is currently an Assistant Professor with the Electrical Engineering Department, King Saud University. His research interests include distributed signal processing, sensor networks, artificial intelligence, and MIMO wireless communication systems.

MAJID ALTAMIMI (S'07–M15) received the B.Sc. (Eng.) degree (Hons.) in electrical engineering from King Saud University, Riyadh, Saudi Arabia, in 2004, the M.A.Sc. degree in 2010, and the Ph.D. degree in electrical and computer engineering from the University of Waterloo, Waterloo, ON, Canada, in 2014. He was a Teaching Assistant with the Department of Electrical and Computer Engineering, University of Waterloo, in 2013. From 2004 to 2006, he was with the Department of Electrical Engineering, King Saud University, where he joined as an Assistant Professor, in 2015. His current research interests include analysis the energy cost for wireless handheld devices and cloud computing architecture, integrate mobile computing with cloud computing, and study and design green information and communications technology solutions.

SALEH A. ALSHEBEILI was the Chairman of the Electrical Engineering Department, King Saud University, from 2001 to 2005. He has over 25 years of teaching and research experience in the area of communications and signal processing. He was a Member of the Board of Directors with the King Abdullah Institute for Research and Consulting Studies, from 2007 to 2009, a member of the Board of Directors with the Prince Sultan Advanced Technologies Research Institute, from 2008 to 2017, where he was the Managing Director, from 2008 to 2011, and the Director of the Saudi-Telecom Research Chair, from 2008 to 2012. He has been the Director of the Technology Innovation Center, RF and Photonics in the e-Society, funded by the King Abdulaziz City for Science and Technology (KACST), since 2011. He is currently a Professor with the Electrical Engineering Department, King Saud University. He has been on the Editorial Board of the *Journal of Engineering Sciences of King Saud University*, from 2009 to 2012. He has also an active involvement in the review process of a number of research journals, KACST general directorate grants programs, and national and international symposiums, and conferences.

• • •